



1

1 **Terrestrial records of glacial terminations V and IV and insights on**
2 **deglacial mechanisms**

3

4 **Fabrizio Marra^{1*}, Alison Pereira^{2,3}, Brian Jicha⁴, Sébastien Nomade⁵, Italo**
5 **Biddittu⁶, Fabio Florindo¹, Giovanni Muttoni⁷, Elizabeth M. Niespolo^{8,9}, Paul**
6 **R. Renne^{8,9}, Vincent Scao⁵**

7 ¹ Istituto Nazionale di Geofisica e Vulcanologia, Rome, Italy

8 ² Université Paris-Saclay, CNRS UMR 8148, GEOPS, France

9 ³ Département Hommes et environnements, Muséum national d'Histoire naturelle,
10 Paris, France

11 ⁴ Department of Geoscience, University of Wisconsin-Madison, USA

12 ⁵ CEA Saclay, LSCE, UMR-8212, UVSQ-IPSL et Université Paris Saclay, Gif-sur-
13 Yvette Cedex, France

14 ⁶ Istituto Italiano di Paleontologia Umana, Anagni, Italy

15 ⁷ Department of Earth Sciences, University of Milan, Milan, Italy

16 ⁸ Department of Earth and Planetary Science, University of California, Berkeley,
17 USA

18 ⁹ Berkeley Geochronology Center, Berkeley, USA

19

20 *Corresponding author: fabrizio.marra@ingv.it

21 ORCID ID [0000-0002-4881-9563](https://orcid.org/0000-0002-4881-9563)

22

23

24 **Abstract**

25 ⁴⁰Ar/³⁹Ar geochronology constraints to aggradational phases and grainsize
26 variations show that the sedimentary filling of the Liri fluvial-lacustrine basin
27 (central Italy) recorded the occurrence of deglaciation events associated with
28 global meltwater pulses.

29 Integrating these data with those from the Tiber River catchment basin, we find a
30 precise match between the ages of gravel deposition and the occurrence of
31 moderate sea-level rise events which anticipate those more marked during the
32 glacial termination V and IV in the Red Sea relative sea level curve.

33 Such correspondence suggests that gravel deposition is facilitated by melting of
34 Apennine mountain range glaciers, which provide the water transport energy
35 and a surplus of clastic input to the rivers draining the mountain regions and
36 flowing into the Tyrrhenian Sea. Therefore, the thick gravel beds intercalated in
37 the sedimentary filling of the catchment basins of the major rivers in central Italy



38 may be regarded as an equivalent proxy of large deglaciation events, similar to
39 the ice-rafted debris in northern Atlantic.
40 Consistent with this hypothesis, we also show the close correspondence between
41 the occurrence of particularly mild (warmer) minima of the mean summer
42 insolation at 65°N and these early aggradational phases, as well as with other
43 anomalous early sea-level rises occurred 750 ka and 540 ka at the onset of
44 glacial termination VIII and VI, and 40 ka at the onset of the so-called Heinrich
45 events.

46

47

48 **Keywords:** glacial termination; aggradational successions; deglacial process;
49 $^{40}\text{Ar}/^{39}\text{Ar}$ geochronology; detrital sanidine

50

51



1. Introduction

Geochronologically constrained independent records of glacial-interglacial variations in ice volume and sea level for the >150 ka interval represent a fundamental tool to decipher Pleistocene global climate evolution. However, records characterized by global significance are very rare (e.g., ocean cores, ice cores, coral reefs, speleothems) and those with direct, precise radioisotopic age constraints, especially in the time interval >500 ka, are even less common. Over 30 years of dedicated studies have shown that fluvial-lacustrine sedimentation within the catchment basin of the Tiber River (Figure 1) responded synchronously with changes in base-level induced by glacio-eustatic fluctuations during Middle-Upper Pleistocene (Alvarez et al., 1996; Karner and Marra, 1998; Karner and Renne, 1998; Marra et al., 1998, 2008, 2013, 2016, 2017a, 2019a, 2021a; Marra and Florindo, 2014; Florindo et al., 2007; Pereira et al., 2020; Giaccio et al., 2021).

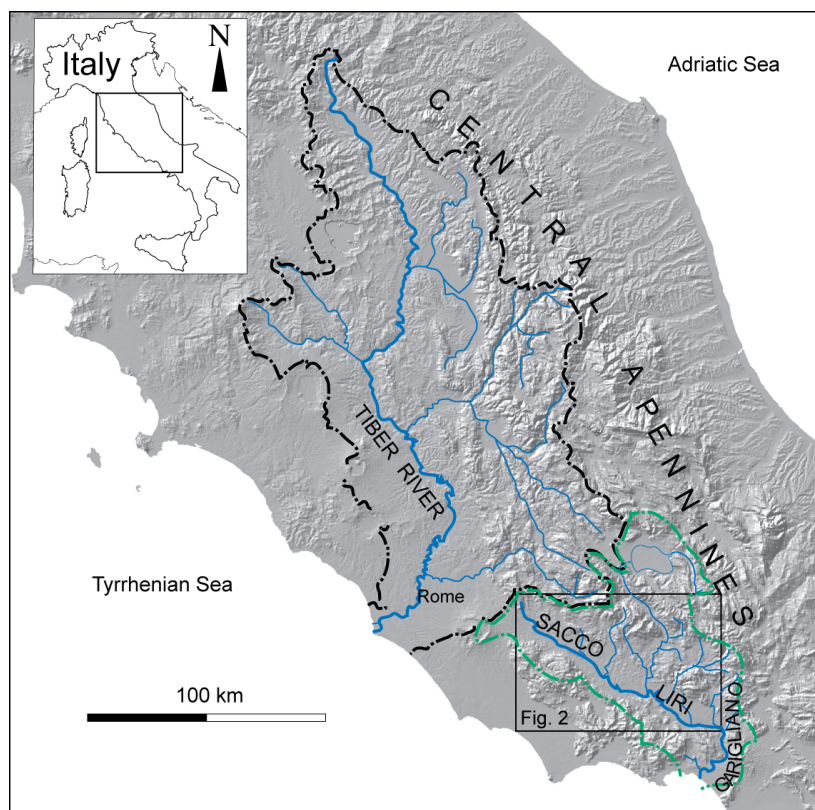




Figure 1 - Catchment basins of the Tiber River and of the Sacco-Liri-Garigliano Rivers. The location of the investigated area represented in Figure 2 is shown. DEM image: TINITALY/01 square WA 6570, used with permission of the Istituto Nazionale di Geofisica e Vulcanologia, Rome.

The sedimentary record of the Paleo-Tiber River consists of a series of fining-upward sequences of clastic sediments deposited above an erosional surface in response to sea-level rise during the last eight glacial-interglacial transitions ('aggradational successions': Karner and Marra, 1998; Marra et al., 2008, 2016, Marra and Florindo, 2014; Luberti et al., 2017). Each sequence is characterized by a basal interval of distinct gravel deposition that abruptly switches to clay deposits. In particular, it has been demonstrated through $^{40}\text{Ar}/^{39}\text{Ar}$ age constraints on tephra layers interbedded with the sedimentary deposits that coarse gravel beds at the base of each aggradational succession are deposited as a consequence of ice-melting during the glacial termination. These works have highlighted that conditions for the accumulation of the coarse gravel deposits only coexisted at the onset of glacial terminations due to several concurrent factors:

- i*- low sea level at glacial maxima, which steepens the gradients and, in turn, enhances the river competence through the more deeply incised valley;
- ii*- melting of Apennine mountain chain glaciers that releases large amount of clastic material, increasing the sediment supply to the river drainage basin;
- iii*- overall increase in regional precipitation.

Gravel starts accumulating at the end of the glacial period, when the continued sea-level fall, which caused re-incision of the valley floor and removal of the gravel transported during the regressive phase through the glacial maximum, terminates. The abruptness of the "sedimentary switch" that marks the transition from the gravel bed (2-8 m in thickness), through a thin (<1 m in thickness) sand bed, into the thick (20-40 m in thickness) silt and clay section claims for the sudden establishment of a low gradient, consistent with fast sea-level rise (meltwater pulse) and subsequent development of a sea-level highstand.

Early works focused on the aggradational successions in the coastal plain and the terminal tract of the Tiber River. More recent studies have highlighted the



103 synchronicity, within uncertainties of age models, between the gravel/clay
104 switch and the peaks of sea-level rise during Marine Isotopic Stage (MIS) 11 and
105 MIS 9 in the higher portion of the Tiber catchment basin, as far inland as 50 km
106 (Giaccio et al., 2021) and 100 km (Marra et al., 2019a) from the coast.
107 Giaccio et al. (2021) have remarked on the coincidence among melt-water pulse
108 events, peaks in the ice-rifted debris (IRD) curve (Barker et al., 2019), and
109 deposition of the gravel beds of the MIS 11 aggradational succession (San Paolo
110 Formation, Karner and Marra, 1998), suggesting that gravel deposition in the
111 catchment basins of the Tiber River can be regarded as an equivalent proxy of
112 deglaciation events. This composite record of radioisotopically dated (^{14}C and
113 $^{40}\text{Ar}/^{39}\text{Ar}$) morpho-sedimentary units can thus provide key geochronological
114 constraints that are generally lacking in the Middle Pleistocene sea-level records,
115 and they can be used to better evaluate the relationship between insolation
116 changes and sea-level oscillations.
117 With these premises in mind, we have investigated the possible response to the
118 glacio-eustatic signal of sediment supply grainsize within the Sacco-Liri-
119 Garigliano Rivers catchment basin, located in central-southern Italy (Figure 1).
120 Here, a more than 50 m thick fluvial-lacustrine succession filled the tectonic
121 depression of the Liri basin during the Middle Pleistocene (Devoto, 1965;
122 Centamore et al., 2010; Marra et al., 2021b). Through $^{40}\text{Ar}/^{39}\text{Ar}$ dating of
123 interbedded volcanic layers, collected both from outcrop and in borehole cores,
124 we provide geochronologic constraints to the sedimentary succession to
125 determine tectonic (uplift/subsidence) rates as well as to pinpoint the time of
126 deposition of two major gravel beds. These are the result of a sudden increase in
127 energy of water transport within the lacustrine basin.

128

129 **2. Geological-structural setting**

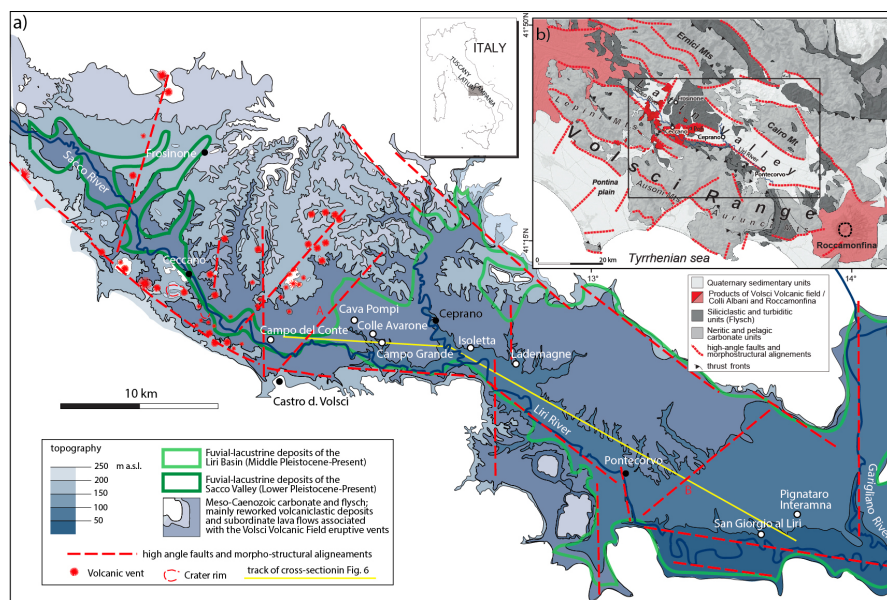
130

131 The Latin Valley (Fig. 2) is part of the central Apennine fold-and-thrust belt,
132 which originated from Late Tortonian-Early Messinian compressional phases
133 and has been affected by extensional tectonics since the Pliocene (Malinverno
134 and Rayan, 1986; Patacca et al., 1990). The outcropping terrains belong to the
135 Latium-Abruzzi neritic carbonate domain (upper Triassic-middle Miocene), and



6

136 are covered by middle Miocene to early Pliocene syn-orogenic siliciclastic
 137 deposits (Centamore et al. 2007, and ref. therein).
 138



139
 140 Figure 2 - a) Morpho-structural sketch of the Latina Valley with the Sacco-Liri catchment basin
 141 showing location of the investigated geologic sections (white dots).
 142 b) Regional geologic map (created by authors) straddling the investigated area.
 143
 144 The study area is organized in several NW-SE striking imbricate thrust sheets
 145 that overthrust onto Tortonian-lower Messinian terrigenous deposits, cross-cut
 146 by a system of conjugated synthetic and antithetic Quaternary normal faults,
 147 which controlled the formation and growth of intramountain basins during the
 148 extensional phase (Cardello et al., 2020, and ref. therein). The articulated
 149 catchment basin of the Sacco, Liri and Garigliano Rivers (Figs. 1 and 2) developed
 150 in a graben structure within the Latina Valley (Cardello et al., 2020).
 151 Locally, the study area has also been affected by N- to NNE- and E- to ENE-
 152 striking high angle faults with strike-slip kinematics up to the Middle Pleistocene
 153 (Sani et al., 2004; Centamore et al., 2010; Cardello et al., 2020). The strike-slip
 154 tectonics have been associated with the eruptive centers of the Volsci Volcanic
 155 Field (Acocella et al., 1996), the activity of which occurred in three main phases
 156 (Marra et al., 2021b, and ref. therein). An early eruptive phase spanning
 157 $761.5 \pm 9.5 - 541.0 \pm 14.0$ ka was characterized by long quiescence periods



158 between isolated eruptive events; a major eruptive activity clustered 424.0 ± 13.0
 159 through 349.5 ± 5.0 ka; finally, a late eruptive phase has poorer geochronologic
 160 constraints between 300.0 ± 28.0 – 231.0 ± 19.0 ka (Marra et al., 2021b).

161

162 **3. Materials and methods**

163 **3.1 Chronostratigraphic analysis**

164 Devoto (1965) described the sedimentary succession filling the large lacustrine
 165 basin in the "Lower Liri Valley", between Ceprano and the Garigliano River
 166 confluence (Fig. 2), as composed of three lacustrine facies with vertical and
 167 lateral transition from one to another:

- 168 i. *Lower lacustrine mud*. Bedded white calcareous muds with frequent black
 169 tephra intercalations.
- 170 ii. *Typical lacustrine facies*. White calcareous muds with alternating cross-bedded
 171 yellow sand layers, black and brown "tuffite" with slumpings, conglomerate.
- 172 iii. *Late lacustrine facies*. Calcareous muds varying in color with occasional lignite
 173 and peat layers, transitioning laterally and vertically to travertine.

174

175 In this study, we investigate three geologic sections (Colle Avarone, San Giorgio
 176 al Liri, Pignataro Interamna) and re-analyze the stratigraphy of six sites
 177 described in the literature (Campo del Conte, Cava Pompei, Campogrande,
 178 Isoletta, Lademagne, Pontecorvo) located in three different structural portions of
 179 the Sacco-Liri basin (Fig. 2). We provide 8 new $^{40}\text{Ar}/^{39}\text{Ar}$ ages both on primary
 180 volcanic samples and reworked deposits containing K-feldspars crystals, which
 181 we integrate with 9 $^{40}\text{Ar}/^{39}\text{Ar}$ and 2 K/Ar dates previously produced from these
 182 sections.

183 Also due to the fact that several geologic sections that are included in this study
 184 are no longer exposed and stratigraphic data have been obtained from the
 185 literature (see Supplementary File #3 for stratigraphic detail), here we adopt a
 186 relatively simple but effective sedimentological approach based on the
 187 identification of three main granulometric classes, aimed at providing
 188 information on the energy of transport and the related sedimentary
 189 environments within the Sacco-Liri catchment basin:



- 190 i. coarse gravel (max diameter of pebbles >2 cm), tractive fluvial environment of
- 191 high transport energy;
- 192 ii. coarse sand with sparse fine gravel (max diameter of pebbles ≤2 cm), fluvial
- 193 environment of mid transport energy;
- 194 iii. silt, clay and carbonate-rich mud; lacustrine and, subordinately, alluvial
- 195 environment of low transport energy.

196
197

198 **3.2 $^{40}\text{Ar}/^{39}\text{Ar}$ analysis**

199 Samples for $^{40}\text{Ar}/^{39}\text{Ar}$ analyses were prepared at the Laboratoire des Sciences du
 200 Climat et de l'Environnement facility (CNRS-CEA, Gif-sur-Yvette), France, and at
 201 the University of Wisconsin-Madison.

202 Three distinct irradiations have been performed and the samples were dated in
 203 three facilities (Berkeley Geochronology Center, USA), Laboratoire des Sciences
 204 du Climat et de l'Environnement (CEA, Gif-sur-Yvette), and WiscAr Laboratory of
 205 Wisconsin University (USA). Samples PO-C6, BL-1A, BL-5, PI-1 and PI-2 were
 206 irradiated in the Cd-lined, in-core CLICIT facility of the Oregon State University
 207 TRIGA reactor.

208 Samples PO-C6, BL-1A and BL-5 were analyzed at the Berkeley Geochronology
 209 Center (BGC; California, USA), using a MAP 215-C mass spectrometer (MAP 1),
 210 following procedures described in Giaccio et al. (2017). Samples BL-4, CE-1, and
 211 CE-2 were analyzed at the University of Wisconsin-Madison (USA), using a
 212 Noblesse 5-collector mass spectrometer, following procedures described in Jicha
 213 et al. (2016). Samples PI-1 and PI-2 were analyzed at LSCE using a VG 5400 mass
 214 spectrometer (LSCE; Gif-sur-Yvette, France), following procedures described in
 215 Pereira et al. (2018).

216 All ages are calculated according to the fluence monitor age of Alder Creek
 217 sanidine (^{40}K total decay constant of Min et al. (2000); $\text{ACs} = 1.1848 \pm 0.0012$ Ma,
 218 Niespolo et al., 2017) and are reported to the precision level of 2σ standard
 219 deviation. Detailed procedures and full $^{40}\text{Ar}/^{39}\text{Ar}$ data are reported in
 220 Supplementary File #1A and #2. Detailed discussion of the results is reported in
 221 Supplementary File #1B.

222



223 3.3 Detrital sanidine dating approach

224 The implemented sensitivity of the modern mass-spectrometers permits to date
 225 with great precision Pleistocene grains smaller than 400–300µm. Combined with
 226 the continuous eruptive activity that characterized the volcanic region of central
 227 Italy during the last 800 ka (Marra et al., 2020, and ref. therein), dating of
 228 sedimentary samples has become an extremely useful tool to assess the ages of
 229 aggradational successions deposited in response to sea-level rise during glacial
 230 terminations in the absence of intercalated, primary tephra layers (see Marra et
 231 al., 2019b for an in-depth discussion). In fact, when a statistically significant
 232 number of crystals is dated (i.e., 30-40 grains), it is reasonable to assume that the
 233 age of the youngest crystal population, besides providing a maximum age for the
 234 sedimentary deposit, should also be regarded as documenting the lack of crystals
 235 from younger eruptive products, implying that no younger eruptions occurred
 236 before the time of deposition. Such assumption consents to consider the
 237 youngest crystal age also an approximate minimum age (*terminus ante-quem*)
 238 (within the recurrence time of the volcanic activity) to the time of deposition of
 239 the sediment. As discussed in Marra et al. (2019b) the youngest eruptions
 240 should be better represented in reworked, sedimentary deposits because their
 241 products crop out in wider areas than the older ones, which are buried under a
 242 longer sequence of strata. This consideration supports the principle that the age
 243 of a layer is bracketed between the ages of its youngest crystal population and of
 244 the next younger eruption, whose crystals do not occur in the layer but is
 245 documented in the area. According to this principle, we will report ages for
 246 reworked samples obtained on the youngest crystal, or weighted mean ages on
 247 the youngest crystal population (2 or more crystals) whenever the case, with the
 248 symbol \leq in the figures of this paper.

249

250 4. Results

251 4.1 $^{40}\text{Ar}/^{39}\text{Ar}$ data

252 Results for the eight samples dated in the present study are described in
 253 Supplementary File #1 and are reported, along with those of 9 previous samples,
 254 as age probability diagrams in Figure 3 and summarized in Table 1. Full
 255 analytical data are reported in Supplementary Material #2.



10

256
257
258
259
260
261

SAMPLE/SITE	Age (ka) $\pm 2\sigma$	n/N	MSWD
BL-5	300 \pm 12	2/17	-
PO-C6	337.5 \pm 6.4	7/23	0.90
CE-2	389.6 \pm 2.7	1/33	-
PI-2	400.9 \pm 3.4	9/11	0.90
PI-1	513.2 \pm 7.4	9/10	0.70
BL-4	516.8 \pm 2.1	28/29	1.04
BL-1A	538.3 \pm 7.0	7/19	0.56
CE-1	452.4 \pm 1.8	1/30	-
from previous literature			
CA-C1 ¹⁴	345.9 \pm 4.3	8/28	0.82
Ceprano ³³	350.6 \pm 8.0	14/17	1.50
CA-CGT ¹⁴	359.6 \pm 6.5	3/24	0.04
Isoletta 3 ²⁷	362.6 \pm 3.8	2/8	0.34
Lademagne 2 ²⁷	386.2 \pm 4.6	7/17	1.60
Isoletta 2 ²⁷	373.2 \pm 2.8	10/13	1.40
Cava Pompi ²⁷	394.3 \pm 8.2	8/8	0.25
Isoletta 1 ²⁷	400.3 \pm 3.0	11/12	0.85
Lademagne 1 ²⁷	402.4 \pm 4.8	7/15	1.10

262 Table 1 - ⁴⁰Ar/³⁹Ar sample ages. All ages according to ACs at 1.1848 Ma (Niespolo
 263 et al., 2017).
 264

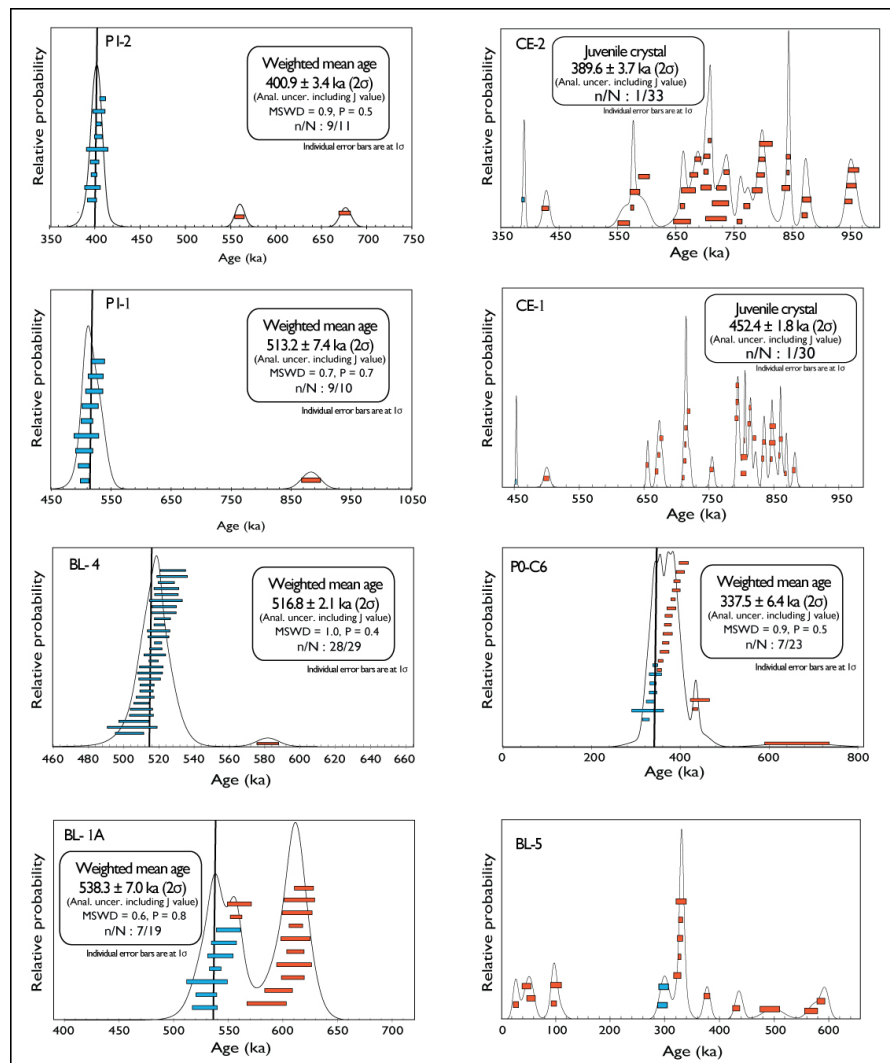


Figure 3 – Results of $^{40}\text{Ar}/^{39}\text{Ar}$ analyses on single crystals from this study presented as probability diagrams.

4.2 Chronostratigraphic analysis of the Sacco-Liri basin

4.2.1 Campo del Conte

A sedimentary sequence about 7 m in thickness, including four fluvial depositional cycles, crops out in the western sector of the Latina Valley in Campo del Conte (Palombo et al., 2000-2002) (Figure 2). This sequence is characterized by the occurrence of *Mammuthus meridionalis* fossils along with those of a cervid belonging to the Pseudo-dama group (Palombo et al., 2000-2002) indicating an



276 Early Pleistocene age. More specifically, *M. meridionalis* lived in central Italy
 277 during the period chronologically framed between 2.6 and 1.6 Ma (Gliozzi et al.,
 278 1997).

279

280 **4.2.1 Campo Grande (Ceprano boreholes)**

281 Two boreholes drilled in the western sector of the Liri basin in Campo Grande
 282 (Fig. 2) recovered 48 m of lacustrine succession between 108 and 60 m a.s.l.,
 283 without reaching its bottom (Muttoni et al., 2009). Three main successions, the
 284 lowest two separated by a ca. 5 m thick gravel layer, were tentatively correlated
 285 with the three lacustrine facies described by Devoto (1965). Although not
 286 strictly applicable everywhere, we will use these three successions, here termed
 287 "lower lacustrine ", "middle lacustrine-fluvial", and "upper fluvial- lacustrine", as
 288 reference chronostratigraphic units in this paper.

289 We have collected two samples from the Campo Grande borecores stored at
 290 Università degli Studi di Milano. Sample CE-1 was collected in borecore Ceprano
 291 1 at 39.3 m depth within a coarse gravel layer with abundant sand matrix. The
 292 youngest crystal out of a population of 30 extracted from this sediment yielded a
 293 $^{40}\text{Ar}/^{39}\text{Ar}$ age of 452.4 ± 1.8 ka. Sample CE-2 was collected at 15.1 m depth in
 294 borehole Ceprano 2, at the base of a coarse sand layer and yielded a youngest
 295 crystal date of 389.6 ± 2.7 ka. As discussed in the previous section, these ages can
 296 be considered good approximations of the time of deposition of these sediments
 297 (see also Suppl. Mat. 1B).

298 Consistent with this hypothesis, a constant sedimentation rate of ~ 38 cm/ky is
 299 calculated from our sample ages combined with that of 350.6 ± 8.0 ka (Nomade et
 300 al., 2011) on the primary volcanic layer cored at the top of the lacustrine
 301 succession (Fig. 4), in good agreement with previous estimation (30-40 cm/ky,
 302 Muttoni et al., 2009). While linear long-term sedimentation rates are likely to
 303 obscure high frequency changes in sediment accumulation as revealed by
 304 sedimentological observations, they provide useful constraints on the
 305 accumulation history of the basin during the overall lifetime of its existence.
 306 Indeed, gravel and cross-bedded sands represent sudden, high-energy inputs
 307 within the lacustrine basin. Also in consideration of their small thickness with
 308 respect to the silty-clayey sediments, the ages of the samples collected in these



13

two horizons may be regarded as good spot constraints to the overall lacustrine sedimentation, which is characterized by relatively constant sedimentation rate. These observations indicate that the ages of 452.4 ± 1.8 ka and 389.6 ± 2.7 ka are excellent time constraints on the deposition of the gravel horizon at the base of the "Middle lacustrine-fluvial succession", and to the start of coarse-sized sedimentary input (cross-bedded sands with sparse gravel) at the base of the "upper fluvial-lacustrine succession".

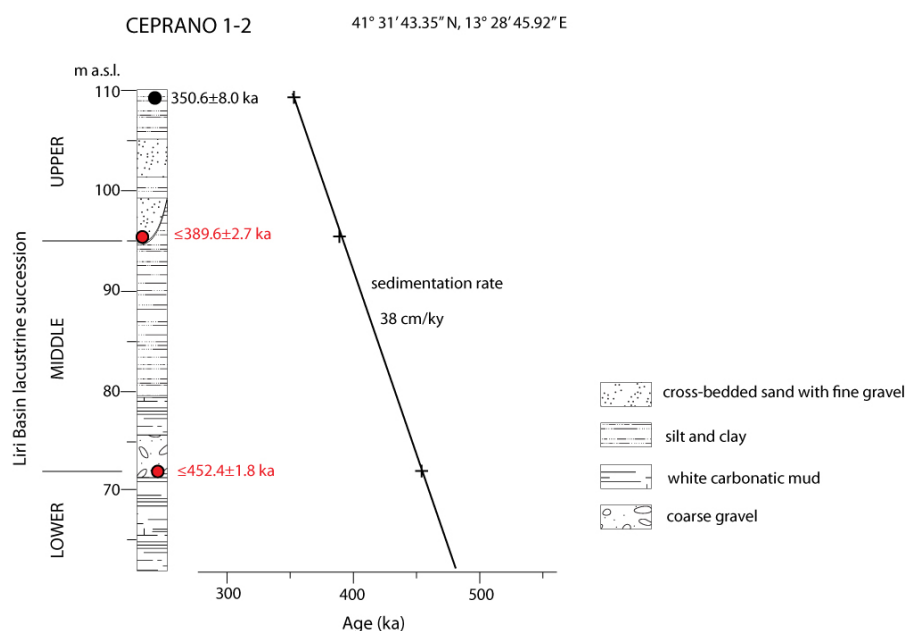


Figure 4 - Synthetic stratigraphic log of the two boreholes drilled in Ceprano (Muttoni et al., 2009) showing the samples dated in the present work (red dots) and in Nomade et al. (2011), which allow to assess the sedimentation rate of the lacustrine succession.

4.2.3 Cava Pompei

Temporary archaeological trench excavations at this location (Biddittu and Segre, 1978) exposed a ca. 3 m thick sedimentary succession overlying a primary pyroclastic-flow deposit (Suppl. Fig. S5). It was constituted, from bottom to top, by a basal, coarse sand-and-gravel volcanoclastic horizon, mostly deriving from reworking of the underlying volcanic deposit. It abruptly passed upwards to bedded, white lacustrine muds and massive, yellowish sandy silt with clay intercalation. A travertine horizon closes the succession.



Lower and upper age constraints to this sedimentary succession are provided by two $^{40}\text{Ar}/^{39}\text{Ar}$ ages performed on the pedogenically altered top horizon of the pyroclastic flow deposit occurring at the base of the succession (Pereira et al., 2018), and on a second, primary volcanic deposit (this work) unconformably overlying it (Suppl. Fig. S5). The lowest sample provides a *terminus post-quem* of 394.3±8.2 ka to the beginning of sedimentation, while the upper sample (PO-C6) gives a *terminus ante-quem* of 337.5±6.4 ka for it.

4.2.4 Colle Avarone

A ca. 8 m thick succession is exposed at several sections at this locality (Suppl. Fig. S6). A coarse gravel in abundant sand-matrix horizon, > 2 m in thickness, occurs at the base and is overlain by a lacustrine succession in which three primary volcanic deposits are intercalated. Two $^{40}\text{Ar}/^{39}\text{Ar}$ ages on one sample (CA-CGT) of sand matrix collected in the basal gravel horizon and on the uppermost pyroclastic-flow deposit (CA-C1) were performed (Marra et al., 2021b), bracketing the deposition of the sedimentary succession between 359.6±6.5 ka and 345.9±4.3 ka.

4.2.5 Isoletta

A more than 30 m-thick section was temporarily exposed during construction of the high-velocity railway in the 90's at this location (Biddittu, 2004). A more than 10 m thick, grey clay and silt lacustrine to fluvial deposit was exposed at the base of the succession, followed by another ca. 10 m thick package of cross-bedded to planar coarse sand (Fig. S7). A ca. 3 m thick layer of coarse gravel follows in the succession, transitioning upwards to sand and silt. A travertineaceous silt horizon closes the succession. Two sub-primary (i.e., reworked in place ashfall deposit) volcanic layers intercalated at the base of the clay and in the middle of the coarse sand horizons provided ages of 400.3±3.0 and 372.2±2.8 ka, respectively (Pereira et al., 2018). A reworked volcanoclastic layer collected in the coarse gravel horizon yielded a youngest population of two crystals providing a *terminus post-quem* age of 362.6±3.8 ka to its deposition (Pereira et al., 2018).



364 4.2.6 Lademagne

365 The sedimentary succession is made up of a 2 m-thick horizon of sand with
 366 abundant medium-to coarse gravel, overlying a clay layer and topped by 1 m of
 367 sandy silt deposits was described at this location (Biddittu et al., 2012). Two sub-
 368 primary volcanoclastic layers collected in the vicinity of the original
 369 archaeological site, which stratigraphically constrain the sedimentary succession
 370 at the bottom and at the top (Suppl. Fig. S8), yielded ages of 402.4 ± 4.8 ka and
 371 386.2 ± 4.6 ka, respectively (Pereira et al., 2018).

372

373

374 4.2.7 Pontecorvo

375 Two tephra layers interbedded in the carbonate-rich muds of the "Lower
 376 Lacustrine Succession" of the Liri basin cropping out in the surroundings of
 377 Pontecorvo village were dated by the K/Ar method at 583 ± 11 ka and 570 ± 11 ka
 378 (Narcisi, 1986; Centamore et al., 2010). We have re-investigated this sector and
 379 detected a geologic section in which several tephra layers occur at elevation
 380 ranging 55-57 m a.s.l. (Suppl. Fig. S9).

381

382 4.2.8 San Giorgio al Liri

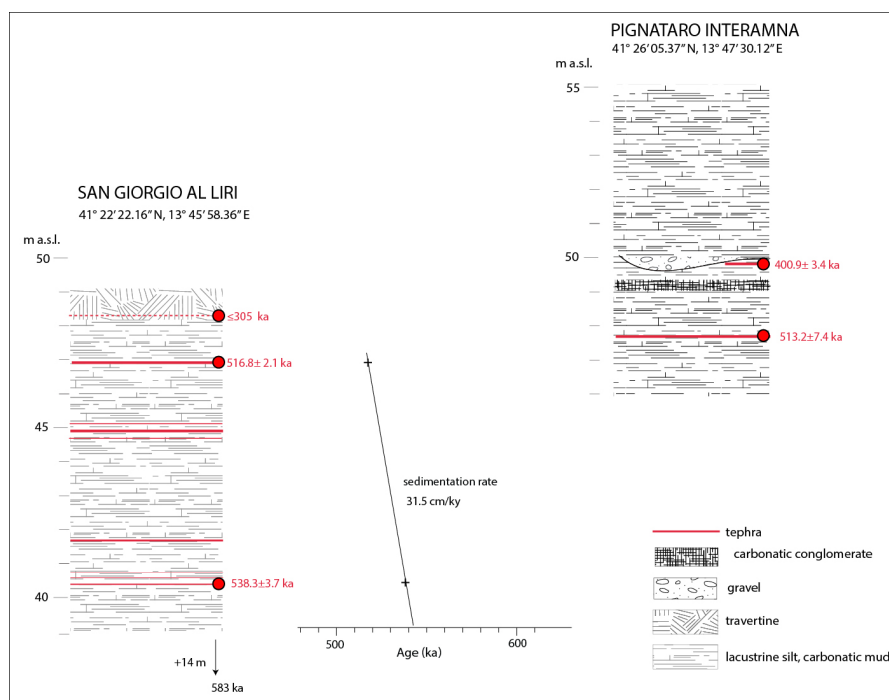
383 A more than 10 m thick succession of white carbonate-rich muds, silts and
 384 travertine layers cropping out in the neighborhoods of San Giorgio al Liri village
 385 has been discovered (Fig. 5a). Eight cm- to dm-thick tephra layers are
 386 intercalated in the lowest 8 m of the succession which is constituted by
 387 lacustrine white carbonate-rich muds. We have dated the lowermost (BL-1A)
 388 and uppermost (BL-4) of these tephra layers, which yielded $^{40}\text{Ar}/^{39}\text{Ar}$ ages of
 389 538.3 ± 7.0 ka and 516.8 ± 2.1 ka, respectively, allowing correlation of the
 390 sedimentary deposits with the "Lower lacustrine succession". In contrast, a
 391 sedimentary sample collected in the travertine horizon at the top of the
 392 succession provided a *terminus post-quem* age of 300 ± 12 ka, evidencing a large
 393 sedimentary hiatus at the top of the lacustrine succession.

394 The ages of the two tephra layers allow an estimate of the sedimentation rate of
 395 ca. 31.5 cm/ky for the lacustrine basin during the corresponding time span.

396



16



397

398

399

400

401

402

403

404

405

406

407

408

409

410

411

412

413

414

415

416

Figure 5 - Stratigraphic sketches of San Giorgio al Liri (a) and Pignataro Interamna (b) sections showing the sampled tephra layers and the average sedimentation rate.

4.2.9 Pignataro Interamna

A more than 20 m thick lacustrine succession crops out in the surroundings of Pignataro Interamna village, which was attributed to the "Typical lacustrine facies" (Devoto, 1965). We have investigated the lowest, 10 m thick portion of this succession cropping out few km southeast of Pignataro Interamna, constituted by white carbonate-rich muds and yellow silts, in which two clastic horizons are intercalated (Fig. 5b). We sampled and dated one primary tephra occurring in the lower part of the lacustrine deposits and the volcanoclastic sand matrix of a discontinuous, up to 20 cm thick gravel layer occurring in the upper portion of the succession. A peculiar, 50 cm thick conglomeratic horizon constituted by poorly rounded, ≤ 1 cm sized carbonate fragments, chert and limestone pebbles within a silty matrix occurs ca. 1.5 m above the lowest tephra layer dated at 513.2 ± 7.4 ka. The maximum age of 400.9 ± 3.4 ka provided by the sample collected in the upper gravel layer, 50 cm above the conglomerate, implies that this clastic horizon marks a significant sedimentary hiatus, similar to



that occurring at the top of the "Lower lacustrine succession" in San Giorgio al Liri. However, more lacustrine deposits occur above this hiatus in Pignataro Interamna, which are a lateral transitional facies of the "upper fluvial-lacustrine succession", as evidenced by the geochronologic constraints provided here.

5. Discussion

5.1 Morphostructural analysis of the Liri basin

Figure 6a shows a NNW-SSE cross-section along the Sacco-Liri valley providing the chrono-stratigraphic correlation of the investigated sections, while a tentative reconstruction of the structural and sedimentary evolution of the Liri lacustrine basin is provided in Figure 7.

Correlation of the sedimentary phases with the stack of globally distributed $\delta^{18}\text{O}$ records (Lisiecki and Raymo, 2005) and the Red Sea relative sea-level (RSL) curve (Grant et al., 2014) is shown in Figure 6b.

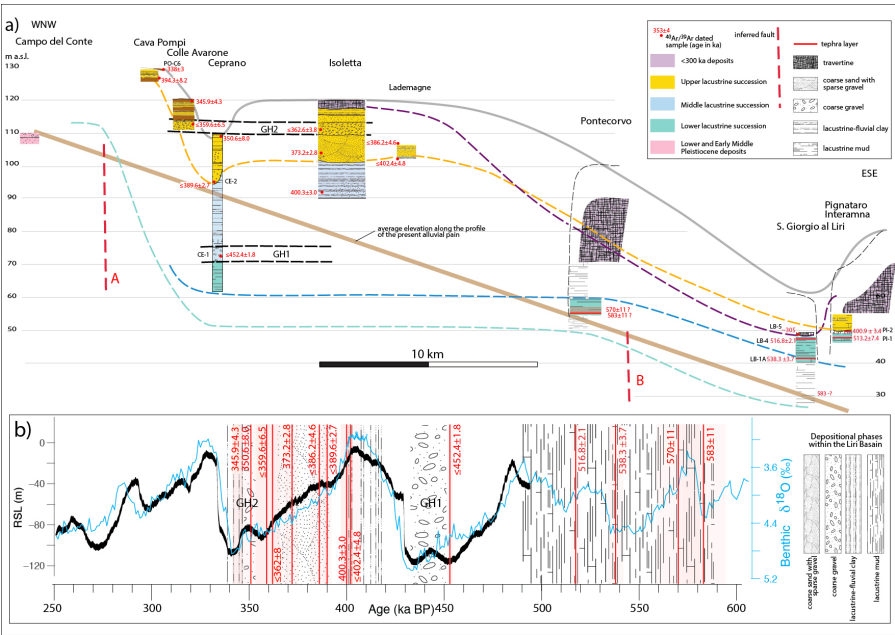


Figure 6 - a) Schematic cross-section along the Liri basin showing the chronostratigraphic correlation of the investigated sections. See text for comments and explanation. b) The age constraints to the sedimentary filling of the Liri basin provided by volcanic layers dated in this and in previous works (vertical red bars; shaded boxes are the 2σ uncertainties) allow comparison of sediment aggradation with the stack of $\delta^{18}\text{O}$ records (Lisiecki and Raymo, 2005) and the relative sea level (RSL) curve (Grant et al., 2014).



439
440 The occurrence of a Lower Pleistocene succession in Campo del Conte at higher
441 elevation with respect to the Middle Pleistocene lacustrine succession in the Liri
442 Basin provides a paleogeographic constraint to the tectonically subsiding sector
443 (inferred fault A in Figures 2 and 7a). Consistent with the present morphology of
444 the Sacco Valley, confined within a narrow incision between the Meso-Cenozoic
445 sedimentary and Middle Pleistocene volcanic terrains (dark green bordered
446 sector in Figure 2), no significant lacustrine sediments occur in this area,
447 showing the absence of tectonic subsidence. In contrast, a more than 50 m thick
448 sedimentary succession spanning in age 450 - 337 ka (middle and upper
449 lacustrine and fluvial successions) occurs in the sector between Cava Pompei and
450 Lademagne, broadly corresponding to the Liri lacustrine basin (light green
451 bordered sector in Figure 2), and overlies more lacustrine sediments (lower
452 lacustrine succession), with ages spanning the 583 - 515 ka interval, at the least
453 (Figure 6a).
454 Taking into account all the abovementioned chrono-stratigraphic constraints, we
455 reconstructed a simplified structural evolution for the Liri Basin (summarized in
456 Figure 7).



19

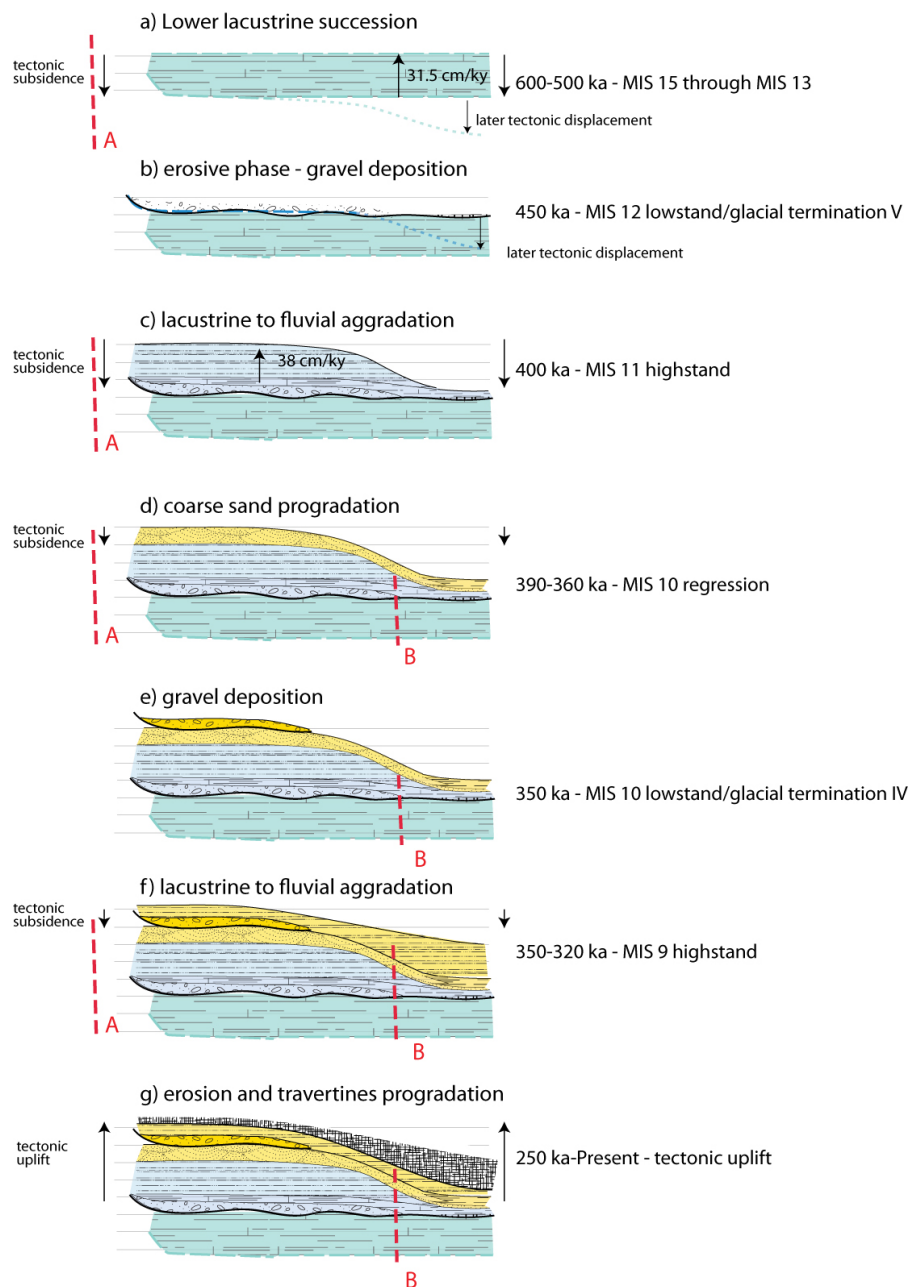


Figure 7 - Proposed stepwise reconstruction of the sedimentary and tectonic evolution of the Liri basin through time. See text for comments and explanations.



463 A lower age constraint to the initiation of the tectonic subsidence of the Liri
464 Basin is not available because the total thickness of the lower lacustrine
465 succession is not known.
466 In Figure 7a, b we have represented only the portion of the lower lacustrine
467 succession which has chronostratigraphic constraints comprised between 583
468 and 515 ka. Given the peculiar sedimentologic features of the lacustrine
469 sediments, represented by carbonate-rich muds which are characteristic of a
470 shallow water environment (Devoto, 1965), this succession should have
471 deposited at relatively constant elevation throughout the Liri basin (Figure 7a).
472 There is no reason to exclude that deposition continued until 500 ka (MIS 13.3
473 highstand, Figure 6b) and that the upper portion of the succession was
474 successively eroded during the MIS 12 regressive phase (Figure 7b), as
475 evidenced by the stratigraphy of the Pignataro Interamna section and by the age
476 constraint of 452.4 ± 1.8 ka (sample CE-1) from the lower gravel horizon in the
477 Ceprano boreholes (GH1 in Fig. 6a).
478 A close relation between the occurrence of MIS 12 lowstand and the deposition
479 of the gravel layer GH1 at the base of the middle lacustrine-fluvial succession is
480 evidenced by the age of sample CE-1 (Fig. 6b). $^{40}\text{Ar}/^{39}\text{Ar}$ constraints to the upper
481 portion of this succession show that rapid aggradation of lacustrine to fluvial
482 clay sediments occurred since the Glacial Termination V, which has an
483 established age of 424 ka (Lisiecki and Raymo, 2005), through 402 ka in
484 response to MIS 11 sea-level rise. The increased sedimentation rate based on the
485 $^{40}\text{Ar}/^{39}\text{Ar}$ age constraints at the Ceprano boreholes is suggestive of enhanced
486 tectonic subsidence in coincidence with the climatic eruptive phase occurred at
487 the Volsci Volcanic Field from 424 through 350 ka (Marra et al., 2021b). Starting
488 from 390 ka, an increase in water transport energy within this sector of the Liri
489 catchment basin resulted in an abrupt sedimentary switch, leading to the
490 deposition of coarse sand with intercalated fine gravel sediments (Fig. 7d; upper
491 fluvial-lacustrine succession). It is followed by the deposition of a 2-3 m thick
492 horizon of well-sorted, coarse gravel, narrowly constrained in the interval
493 350.6 ± 8.0 - 345.9 ± 4.3 ka. This time interval encompasses the whole regressive
494 phase of MIS 10 (Fig. 7e). Another abrupt sedimentary shift into clayey
495 sediments is noted at Colle Avarone and Cava Pompei sections, where lacustrine



496 deposits overly the coarse gravel horizons (Fig. 7f). However, thickness of the
 497 fine-grained portion of the upper fluvial-lacustrine succession is very limited and
 498 it passes upwards to wide travertine plateaus characterized by very thick
 499 deposits to the southeast (Devoto, 1965) (Fig. 7g).

500 We correlate this sedimentary change to the decrease/cessation of the tectonic
 501 subsidence in the Liri Basin, which may be due to the vanishing of the volcanic
 502 activity at the Volsci Volcanic Field (VVF) since 350 ka. Published ages of the VVF
 503 spanning 300-200 ka are poorly constrained, with the youngest reliable eruption
 504 age that of the Colle Borrello center occurring at 331.6 ± 3.0 ka (Marra et al.,
 505 2021b). The lack of a fine-grained aggradational succession deposited during
 506 MIS 9 highstand (337 - 325 ka, Fig. 6b) is likely related to the tectonic inversion
 507 within the Liri Basin.

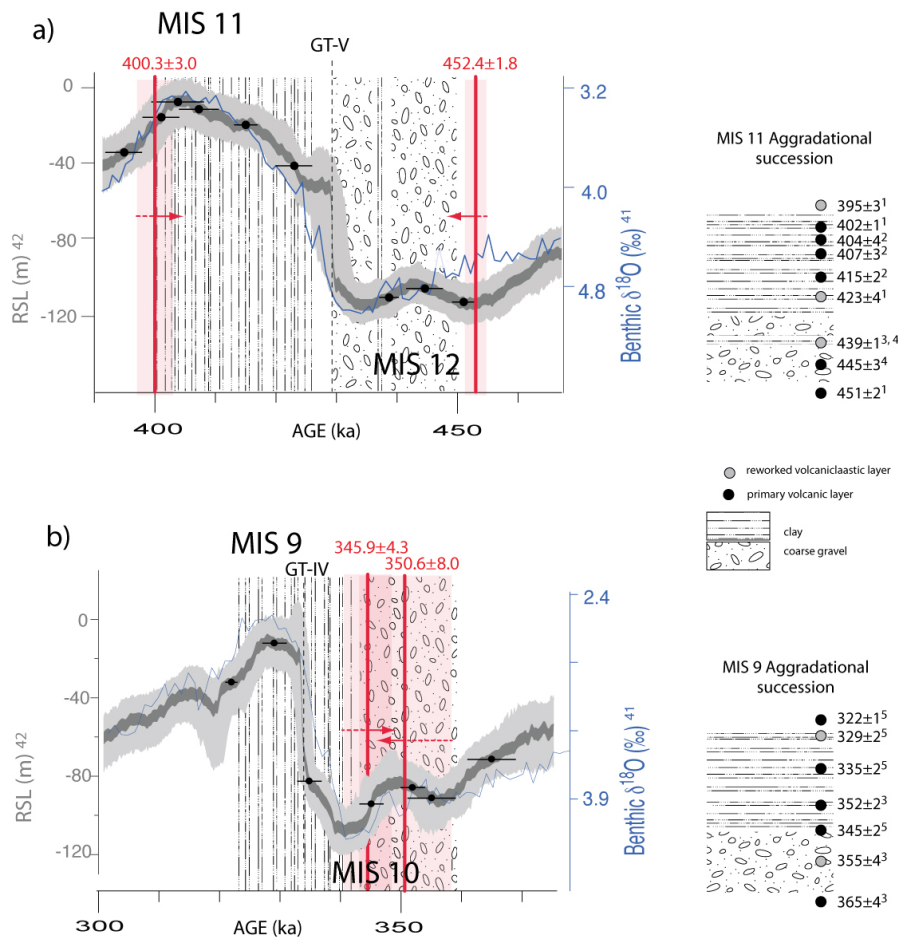
508 Evidence for deep erosion of the upper fluvial-lacustrine succession occurs at
 509 San Giorgio al Liri section, where travertine deposits directly overlying the lower
 510 lacustrine succession yielded a *terminus post-quem* age of 310 ± 12 ka, consistent
 511 with occurrence of the regressive phase of MIS 8 since 320 ka (Fig. 6b).

512 Contextual erosion and travertine progradational deposition is likely to have
 513 occurred throughout MIS 8, 320 - 270 ka (Fig. 6b), while the origin of a series of
 514 terraced paleo-surfaces throughout the Liri Basin is referable to the following
 515 regional uplift phase. Indeed, according to several authors (Karner et al., 2001;
 516 Ferranti et al., 2006; Marra et al., 2016b, 2017b, 2019b), the Tyrrhenian Sea
 517 Margin of central Italy underwent a variable uplift of several tens of meters in
 518 the last 250 ka.

519
 520
 521
 522
 523
 524
 525
 526
 527
 528



529 **5.2 Relationships between sediment grainsize and sea-level fluctuations**
530



531
532 Figure 8 - $^{40}\text{Ar}/^{39}\text{Ar}$ age constraint to sediment aggradation in the Liri basin (red vertical bars)
533 for (a) MISs 11–12 across Glacial Termination V, and (b) MISs 9–10 across Glacial Termination IV
534 are compared to those provided in previous works to the aggradational successions of the Paleo-
535 Tiber River reported in the stratigraphic sections to the right (1: Marra et al., 2021a; 2: Pereira et
536 al., 2020; 3: Marra et al., 2016a; 4: Giaccio et al., 2021; 5: Marra et al., 2019a). Red arrows
537 pointing to the left indicate terminus post-quem (maximum) ages and those pointing to the right
538 indicate terminus ante-quem (minimum) ages. See text for comments and explanation.
539

541 The $^{40}\text{Ar}/^{39}\text{Ar}$ constraints provided here to the deposits of the middle lacustrine
542 succession bracket their deposition in the interval 452.4±1.8 - 400.3±3.0 ka,
543 demonstrating that they correspond to an aggradational succession *sensu*⁹. In
544 other words, the dated morpho-sedimentary unit formed in response to sea-level
545 rise during the glacial-interglacial transition.



546 The complete chronostratigraphic record of the MIS 11 aggradational succession
 547 occurring in the coastal setting (San Paolo Formation, Karner and Marra, 1998;
 548 Marra et al., 2016a, 2021a; Pereira et al., 2020; Giaccio et al., 2021) reported in
 549 Figure 8a shows that the equivalent deposit of the Liri Basin provides identical
 550 age constraints to the deposition of the basal gravel layer and to the completion
 551 of aggradation of the fine-grained sedimentary package, between 450 and 400
 552 ka.

553 Remarkably, Giaccio et al. (2021) demonstrated the early aggradation of a first
 554 gravel layer at 443.1 ± 3.2 ka before the onset of Glacial Termination V and
 555 coinciding with a minor sea-level rise on the RSL curve (Grant et al., 2014) (Fig.
 556 8a). Following this event, another gravel layer passing upwards to a thick clay
 557 succession was deposited after 437.1 ± 1.2 ka, in good agreement with the timing
 558 of the glacial termination and the sea-level rise at the onset of MIS 11 highstand
 559 (Fig. 8a). Giaccio et al. (2021) interpreted the early aggradation phase during MIS
 560 12 as a first meltwater pulse (MWP1) event, preceding the larger amplitude
 561 meltwater pulse during Glacial Termination V (MPW2). These authors remarked
 562 that both MWPs coincide with episodes of ice-rafted debris deposition in the
 563 North Atlantic (Heinrich-like events, Hemming, 2004) and with attendant
 564 Southern Hemisphere warming, plausibly associated with the bipolar seesaw.
 565 Indeed, the occurrence of prominent ice-rafted debris (IRD, Barker et al., 2019)
 566 peaks associated with these meltwater pulses alludes to episodes of extensive
 567 iceberg calving in the North Atlantic, consistent with sustained melting of the
 568 circum-North Atlantic ice sheets (Mc Manus et al., 1999) during these events.
 569 The age of 452.4 ± 1.8 ka, which constrains the start of gravel deposition in the
 570 Liri Basin, provides strong indication of coarse clastic input to the river
 571 catchments of the Tyrrhenian Sea margin deriving from early deglaciation in the
 572 Apennines mountain range. It also provides further evidence for the validity of
 573 the sedimentary model of the "aggradational successions" (Marra et al., 2008,
 574 2016a).

575 The reasons for such a far field response also rely in the lesser elevation gain
 576 within the catchment basin, which has been successively increased by regional
 577 uplift over the last 250 ka (Karner et al., 2001; Ferranti et al., 2006; Marra et al.,
 578 2016b, 2017b, 2019b). In contrast, a comparison of the average uplift rate in the



last 250 ka (0.24 mm/yr) with the average sedimentation rate during the aggradational phases (e.g., 2.3 mm/yr) suggests that glacio-eustasy overrides the tectonic effects, which only impact the accommodation space, and, in turn, the total thickness (rather than the timing of deposition) of each aggradational succession (Marra et al., 2019a).

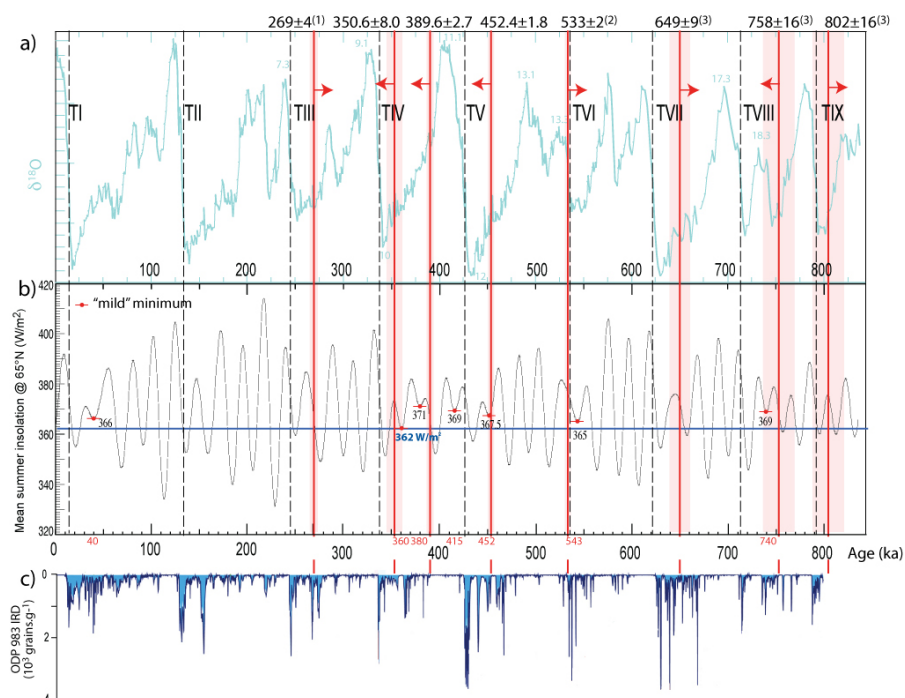
The early aggradation of the MIS 9 sedimentary record (Aurelia Formation, Karner and Marra, 1998) was evidenced (Marra et al., 2016a) and it has been constrained further by successive work (Marra et al., 2019a). In particular, a primary volcanic deposit dated at 345 ± 3 ka at the top of the basal gravel bed of the MIS 9 aggradational succession in the upper sector of the Tiber River catchment basin (Marra et al., 2019a) (Figure 8b) provided a *terminus ante-quem* for its deposition, preceding the canonical age of 337 ka (Lisiecki and Raymo, 2005) for Glacial Termination IV. The narrow age constraints to the second gravel layer occurring in the upper lacustrine succession in the Liri Basin provide a striking match with those provided in the coastal and more inner sectors of the Tiber River basin (Karner and Renne, 1998; Marra et al., 2016a, 2019a), evidencing an early deglaciation occurring during MIS 10 (Fig. 8b). Remarkably, this early aggradational phase also corresponds with a minor sea-level rise in the RSL curve preceding the glacial termination (Fig. 8b), suggesting the same triggering mechanism (i.e., early ice melting) as that hypothesized for the analogous eustatic event during MIS 12.

5.3 Possible triggering mechanisms to deglaciation

Associated with the introduction of the aggradational successions model, Marra et al. (2016a) proposed a possible forcing mechanism based on the occurrence of particularly mild insolation minima which may be regarded as the pre-conditioning factor to trigger a glacial termination. We re-propose this notion in Figure 9, based on the comparison of the two geochronologically constrained sedimentary records of glacial terminations V and IV provided in this paper with the mean summer insolation curve at 65°N (Laskar, 2004).



25



610

611 Figure 9 - $^{40}Ar/^{39}Ar$ age constraints (vertical red bars, shaded boxes are the 2σ uncertainties) to
 612 the coarse gravel beds occurring in the sedimentary filling of the Liri basin provided in this work,
 613 as well as at the base of the aggradational successions of the Paleo-Tiber River provided in
 614 previous studies (1, 2: Marra et al., 2016a, 2017a; 3: Marra and Florindo, 2014). Red arrows as in
 615 Fig. 8. a) Comparison with the glacial termination (GT) ages established through the calibration
 616 of the $\delta^{18}O$ curve (Lisiecki and Raymo, 2005); b) comparison with a set of "mild" minima (see text
 617 for explanation) of the mean summer insolation curve at 65°N (Laskar, 2004); c) comparison
 618 with the ice-rafted debris (IRD) record of core ODP 983 (Barker et al., 2019).
 619

620 The interval 450-359 ka encompassing the two glacial terminations investigated
 621 in this paper is characterized by the occurrence of four such "mild" minima.
 622 Indeed, if we consider the insolation value of 362 W/m² for the insolation
 623 minimum occurring at 360 ka as a lower threshold (blue horizontal line in Figure
 624 9), we see that only six other minima were characterized by higher insolation,
 625 whereas all other minima in the last 800 ky were "colder". These six mild
 626 (warmer) minima are all associated with evidence of anomalous meltwater pulse
 627 events. The oldest one (369 W/m²), at 740 ka, is associated with the early
 628 emplacement at ca. 750 ka of a thick gravel layer in the Paleo-Tiber delta, which
 629 was interpreted as a previously unrecognized glacial termination (i.e., MIS 18.3,
 630 TVIII-A, Marra et al., 1998, 2008). Remarkably, the second oldest mild minimum



at 543 ka is associated with an identical feature of the $\delta^{18}\text{O}$ curve: a double isotopic peak. However, the only difference in this case is that the earliest peak (13.3) is associated in the literature with the eustatic event which is considered the true glacial termination VI, as opposed to MIS 17, for which the glacial termination has been associated with the younger 17.3 peak (Lisiecki and Raymo, 2005) (Fig. 9). Unfortunately, the lack of a detailed record of RSL in the interval >500 ka hinders the possibility to verify if both these mild minima actually preceded meltwater pulses.

In contrast, a striking coincidence between the mild minima at 452 and 360 ka and the early aggradational phases during MIS 12 and MIS 10, which are associated with the emplacement of the coarse gravel beds at ~453 and ~351 ka in the catchment basins of the Tiber and of the Sacco-Liri rivers, is evident by inspection of Figure 9. A lesser of such events is also clearly associated with the mild minimum of 371 W/m^2 occurring at 380 ka, which triggered the grainsize inversion in the Liri Basin causing the emplacement of the coarse sand-and fine gravel horizon which has a *terminus post-quem* age of 390 ± 1 ka.

Moreover, the most outstanding observation is that the only other mild minima of 366 W/m^2 in the last 350 ka occurred at 40 ka, in close connection with the onset of the Heinrich events (Hemming, 2004).

This is strong supporting evidence for relating the early aggradational phases responsible for the emplacement of gravel beds in the Tiber and Liri basins with deglaciation events (meltwater pulses) that triggered relatively minor sea-level rises, and which represent the equivalent of past Heinrich-like events in the Apennines of central Italy.

655

656 Conclusions

$^{40}\text{Ar}/^{39}\text{Ar}$ geochronology provided in this paper, used to constrain the aggradational phases and grainsize variations of the sedimentary filling of the Liri fluvial-lacustrine basin, provide outstanding evidence to support the "aggradational successions" model (Marra et al., 2008, 2016a; Giaccio et al., 2021) as a powerful tool to detect with great detail the occurrence of deglaciation events that triggered global meltwater pulses.



663 We demonstrate a substantial synchronicity between the ages of gravel
664 deposition in both the Tiber and Liri rivers catchment basins and the occurrence
665 of moderate sea-level rise events, which anticipate those more marked during
666 the glacial terminations V and IV in the Red Sea relative sea level curve (Grant et
667 al., 2014).

668 We also show a striking correspondence among the occurrence of particularly
669 mild (warmer) minima of the mean summer insolation at 65°N (Laskar, 2004)
670 and these early aggradational phases, as well as with other anomalous early sea-
671 level rises occurring at the onset of glacial terminations VIII and VI, and at 40
672 ka at the onset of the so-called Heinrich events (Hemming, 2004).

673 Such correspondences suggest that gravel deposition is triggered by melting of
674 the Apennines mountain range glaciers, providing the water transport energy
675 and a surplus of clastic input in the catchment basins of the rivers draining the
676 mountain regions and flowing into the Tyrrhenian Sea. Such
677 hydrologic/sedimentary processes, which occur in any mountain region of the
678 globe, if correctly depicted and dated, can provide a large dataset of deglaciation
679 proxies to unravel the chronology of glacio-eustatic events occurring in the last 1
680 Ma.

681

682

683 **Declaration of competing interests**

684 The authors declare no conflicts of interest.

685

686 **Data availability**

687 ⁴⁰Ar/³⁹Ar full analytical data are available in Supplementary Data File #2.

688

689 **Funding**

690 This research received no funding.

691

692

693



694 REFERENCES

- 695
 696 Acocella, V., Faccenna, C., & Funicello, R. (1996). Elementi strutturali della media
 697 Valle Latina. *Bollettino Società Geologica Italiana*, 115, 501-518.
 698
 699 Alvarez, W., Ammerman, A.J., Renne, P.R., Karner, D.B., Terrenato, N., Montanari,
 700 A., 1996. Quaternary fluvial-volcanic stratigraphy and geochronology of the
 701 Capitoline hill in Rome. *Geology* 24, 751-754.
 702
 703 Barker, S., Knorr, G., Conn, S., Lordsmith, S., Newman, D., & Thornalley, D. (2019).
 704 Early interglacial legacy of deglacial climate instability. *Paleoceanography and*
 705 *Paleoclimatology*, 34, 1455–1475. <https://doi.org/10.1029/2019PA003661>
 706
 707 Biddittu, I., 2004. Guida del Museo Preistorico di Pofi. Quaderni di Argyl 1.
 708 Regione Lazio, Amministrazione provinciale di Frosinone, Comune di Pofi.
 709
 710 Biddittu, I., Segre, A.G., 1978. Paleolitico inferiore a Cava Pompei presso Pofi,
 711 Frosinone. *Quaderni Centro Studi Arch. Etrusco-Ital.* 1, 78-79.
 712
 713 Biddittu, I., Canetri, E., Commerci, V., Germani, M., Picchi, G., 2012. Nuove ricerche
 714 nel giacimento del Paleolitico inferiore di Lademagne, S. Giovanni Incarico
 715 (Frosinone) in *Lazio e Sabina 9* (ed. Ghini, G. & Mari, Z.) 437-443 (Edizioni
 716 Quasar, 2012).
 717
 718 Cardello G.L., Consorti L., Palladino D.M., Carminati E., Carlini M., & Doglioni C.
 719 (2020). Tectonically controlled carbonate-seated maar-diatreme volcanoes: The
 720 case of the Volsci Volcanic Field, central Italy. *J. Geodyn.*, 139, 101763.
 721
 722 Centamore, E., Di Manna, P., & Rossi, D. (2007). Kinematic evolution of the Volsci
 723 Range: a new overview. *Italian Journal of Geosciences* 126, 159–172.
 724
 725 Centamore, E., Dramis, F., Di Manna, P., Fumanti, F., Milli S., Rossi, D., Palombo,
 726 M.R., Palladino, D.M., Trigila, R., Zanon, V., Chiochini, M., Didaskalou, P., Potetti,
 727 M., & Nisio, S. (2010). Note illustrative del Foglio 402 Ceccano. Carta Geologica
 728 d'Italia 1:50.000. Servizio Geologico d'Italia, Roma.
 729
 730 Devoto, G., 1965. Lacustrine Pleistocene in the lower Liri Valley (southern
 731 Latium). *Geologica Romana* 4, 291–368.
 732
 733 Ferranti, L., Antonioli, F., Mauz, B., Amorosi, A., Dai Pra, G., Mastronuzzi, G.,
 734 Monaco, C., Orrù, P., Pappalardo, M., Radtke, U., Renda, P., Romano, P., Sansò, P.,
 735 Verrubbi, V., 2006. Markers of the last interglacial sea-level high stand along the
 736 coast of Italy: Tectonic implications. *Quaternary International* 145/146, 30-54.
 737
 738 Florindo, F., Karner, D.B., Marra, F., Renne, P.R., Roberts A.P., Weaver, R., 2007.
 739 Radioisotopic age constraints for Glacial Terminations IX and VII from
 740 aggradational sections of the Tiber River delta in Rome, Italy. *Earth and*
 741 *Planetary Science Letters* 256, 61-80. doi: 10.1016/j.epsl.2007.01.014.
 742



- 743 Giaccio, B., Niespolo, E., Pereira, A., Nomade, S., Renne, P.R., Alber, P.G., Arienzo, I.,
 744 Regattieri, Wagner, B., Zanchetta, G., Gaeta, M., Galli, P., Mannella, G., Peronace, E.,
 745 Sottili, G., Florindo, F., Leicher, N., Marra, F., Tomlinson, E.L., 2017. First
 746 integrated tephrochronological record for the last ~190 kyr from the Fucino
 747 Quaternary lacustrine succession, central Italy. *Quaternary Science Reviews* 158,
 748 211-234. <http://dx.doi.org/10.1016/j.quascirev.2017.01.004>
 749
- 750 Giaccio, B., Marino, G., Marra, F., Monaco, L., Pereira, A., Zanchetta, G., Gaeta, M.,
 751 Leicher, N., Nomade, S., Palladino, D.M., Sottili, G., Guillou, H., Scao, V., 2021.
 752 Tephrochronological constraints on the timing and nature of sea-level change
 753 prior to and during glacial termination V. *Quaternary Science Reviews*,
 754 <https://doi.org/10.1016/j.quascirev.2021.106976>
 755
- 756 Gliozzi, E., Abbazzi, L., Argenti, P., Azzaroli, A., Caloi, L., Capasso Barbato, L., Di
 757 Stefano, G., Esu, D., Ficarelli, G., Girotti, O., Kotsakis, T., Masini, F., Mazza, P.,
 758 Mezzabotta, C., Palombo, M.R., Petronio, C., Rook, L., Sala, B., Sardella, R., Zanalda,
 759 E., Torre, D., 1997. Biochronology of selected mammals, molluscs and ostracods
 760 from the middle Pliocene to the late Pleistocene in Italy. *Riv. Ital. Paleontol.*
 761 *Stratigr.* 103, 369-388.
 762
- 763 Grant, K.M., Rohling, E.J., Ramsey, C.B., Cheng, H., Edwards, R.L., Florindo, F.,
 764 Heslop, D., Marra, F., Roberts, A.P., Tamisiea, M.E., Williams, F., 2014. Sea-level
 765 variability over five glacial cycles. *Nature Communications* 5, 5076.
 766 doi:10.1038/ncomms6076
 767
- 768 Hemming, S. R., 2004. Heinrich events: Massive late Pleistocene detritus layers of
 769 the North Atlantic and their global climate imprint. *Reviews of Geophysics* 42,
 770 RG1005. doi:10.1029/2003RG000128.
 771
- 772 Jicha, B.R., Singer, B.S. & Sobol, P. Re-evaluation of the ages of $^{40}\text{Ar}/^{39}\text{Ar}$ sanidine
 773 standards and supereruptions in the western U.S. using a Noblesse multi-
 774 collector mass spectrometer. *Chemical Geology* 431, 54-66 (2016).
 775
- 776 Karner, D.B., Marra, F., 1998. Correlation of fluviodeltaic aggradational sections
 777 with glacial climate history: A revision of the Pleistocene stratigraphy of Rome.
 778 *Geological Society of America Bulletin* 110, 748-758.
 779
- 780 Karner, D.B., Renne, P.R., 1998. $^{40}\text{Ar}/^{39}\text{Ar}$ geochronology of Roman volcanic
 781 province tephra in the Tiber River valley: Age calibration of middle Pleistocene
 782 sea-level changes. *Geological Society of America Bulletin* 110, 740-747.
 783
- 784 Karner, D.B., Marra, F., Florindo, F., Boschi, E., 2001. Pulsed uplift estimated from
 785 terrace elevations in the coast of Rome: Evidence for a new phase of volcanic
 786 activity? *Earth and Planetary Science Letters* 188, 135-148.
 787
- 788 Laskar, J., Robutel, P., Joutel, F., Gastineau, M., Correia, A. C. M., Levrard, B., 2004.
 789 A long-term numerical solution for the insolation quantities of the
 790 Earth. *Astronomy & Astrophysics* 428, 261-285.
 791



- 792 Lisiecki, L.E., Raymo, M.E., 2005. A Pliocene-Pleistocene stack of 57 globally
793 distributed benthic $d^{18}O$ records. *Paleoceanography* 20, PA1003.
794 <http://dx.doi.org/10.1029/2004PA001071>.
795
- 796 Luberti, G.M., Marra, F., Florindo, F., 2017. A review of the stratigraphy of Rome
797 (Italy) according to geochronologically and paleomagnetically constrained
798 aggradational successions, glacio-eustatic forcing and volcano-tectonic
799 processes. *Quaternary International*, 438, 40-67.
800 <http://dx.doi.org/10.1016/j.quaint.2017.01.044>
801
- 802 Malinverno, A., Ryan, W.B.F., 1986. Extension in the Tyrrhenian sea and
803 shortening in the Apennines as results of arc migration driven by sinking of the
804 lithosphere. *Tectonics* 5, 227-245.
805
- 806 McManus, J. F., Oppo, D. W., & Cullen, J. L. (1999). A 0.5 - million - year record of
807 millennial - scale climate variability in the North Atlantic. *Science*, 283(5404),
808 971-975.
809
- 810 Marra, F., Florindo, F., 2014. The subsurface geology of Rome: Sedimentary
811 processes, sea-level changes and astronomical forcing. *Earth-Science Reviews*
812 136, 1-20.
813
- 814 Marra, F., Florindo, F., Karner, D.B., 1998. Paleomagnetism and geochronology of
815 early Middle Pleistocene depositional sequences near Rome: comparison with the
816 deep sea $d^{18}O$ climate record. *Earth and Planetary Science Letters*, 159, 147-164.
817
- 818 Marra, F., Florindo, F., Boschi, E., 2008. History of glacial terminations from the
819 Tiber River, Rome: Insights into glacial forcing mechanisms. *Paleoceanography*
820 23, 1-17. doi:10.1029/2007PA001543
821
- 822 Marra, F., Bozzano, F., Cinti, F.R., 2013. Chronostratigraphic and lithologic
823 features of the Tiber River sediments (Rome, Italy): implications on the Post-
824 glacial sea-level rise and Holocene climate. *Global and Planetary Change*.
825 <https://doi.org/10.1016/j.gloplacha.2013.05.002>
826
- 827 Marra, F., Rohling, E.J., Florindo, F., Jicha, B., Nomade, S., Pereira, A., Renne, P.R.,
828 2016a. Independent $40Ar/39Ar$ and $14C$ age constraints on the last five glacial
829 terminations from the aggradational successions of the Tiber River, Rome (Italy).
830 *Earth Planet Sci. Lett.* 449, 105-117. doi:10.1016/j.epsl.2016.05.037
831
- 832 Marra, F., Florindo, F., Anzidei, M., & Sepe, V., 2016b. Paleo-surfaces of glacio-
833 eustatically forced aggradational successions in the coastal area of Rome:
834 assessing interplay between tectonics and sea-level during the last ten
835 interglacials. *Quaternary Science Reviews* 148, 85-100.
836 <http://dx.doi.org/10.1016/j.quascirev.2016.07.003>
837
- 838 Marra, F., Jicha, B., Florindo, F., 2017a. $40Ar/39Ar$ dating of Glacial Termination
839 VI: constraints to the duration of Marine Isotopic Stage 13. *Scientific Reports* 7,
840 8908. doi:10.1038/s41598-017-08614-6



- 841
 842 Marra, F., Florindo, F., Petronio, C., 2017b. Quaternary fluvial terraces of the
 843 Tiber Valley: geochronologic and geometric constraints on the back-arc
 844 magmatism-related uplift in central Italy. *Journal Scientific Reports* 7: 2517.
 845 DOI:10.1038/s41598-017-02437-1
 846
 847 Marra, F. Costantini, L., Di Buduo, G.M. Florindo, F., Jicha, B.R., Monaco, L.,
 848 Palladino, D.M., Sottili, G., 2019a. Combined glacio-eustatic forcing and volcano-
 849 tectonic uplift: geomorphological and geochronological constraints on the Tiber
 850 River terraces in the eastern Vulsini Volcanic District (central Italy). *Global and*
 851 *Planetary Change* 182,103009. doi:10.1016/j.gloplacha.2019.103009.
 852
 853 Marra, F. Gaeta, M. Jicha, B.R. Nicosia, C. Tolomei, C. Ceruleo, P. Florindo, F. Gatta,
 854 M. La Rosa, M. Rolfo, M.F., 2019b. MIS 9 to MIS 5 terraces along the Tyrrhenian
 855 Sea coast of Latium (central Italy): assessing interplay between sea-level
 856 oscillations and tectonic movements, *Geomorphology* 346: 106843.
 857 DOI:10.1016/j.geomorph.2019.106843
 858
 859 Marra, F., Castellano, C., Cucci, L. Florindo, F., Gaeta, M., Jicha, B., Palladino, D.M.,
 860 Sottili, G., Tertulliani, A., Tolomei, C., 2020. Monti Sabatini and Colli Albani: the
 861 dormant twin volcanoes at the gates of Rome, *Scientific Reports* 10(1), 8666.
 862
 863 Marra, F., Pereira, A., Boschian, G., Nomade, S., 2021a. MIS 13 and MIS 11
 864 aggradational successions of the Paleo-Tiber delta: geochronological constraints
 865 to sea-level fluctuations and to the Acheulean sites of Castel di Guido and
 866 Malagrotta (Rome, Italy), *Quaternary International*
 867
 868 Marra, F., Cardello, L., Gaeta, M., Jicha, B., Montone, P., Niespolo, E., Nomade, S.,
 869 Palladino, D.M., Pereira, A., De Luca, G., Florindo, F., Frepoli, A., Renne, P., Sottili,
 870 G., 2021b. The Volsci Volcanic Field (central Italy): an open window on
 871 continental subduction processes, *International Journal of Earth Sciences*
 872 110:689–718. DOI:10.1007/s00531-021-01981-6
 873
 874 Min, K., Mundil, R., Renne, P. R., & Ludwig, K. R. A test for systematic errors in
 875 $^{40}\text{Ar}/^{39}\text{Ar}$ geochronology through comparison with U/Pb analysis of a 1.1-Ga
 876 rhyolite. *Geochimica et Cosmochimica Acta* 64, 73–98 (2000).
 877
 878 Muttoni, G., Scardia, G., Kent, D. V. D, Swisher, C. C. & Manzi, G. Pleistocene
 879 magnetochronology of early hominin sites at Ceprano and Fontana Ranuccio,
 880 Italy. *Earth and Planetary Science Letters* **286**, 255-268 (2009).
 881
 882 Narcisi, B, 1986. Ricerche di tefracronologia nella media e bassa Valle Latina.
 883 *Mem Soc Geol It* 35, 909–912.
 884
 885 Niespolo, E. M., Rutte, D., Deino, A. L., Renne, P. R., 2017. Intercalibration and age
 886 of the Alder Creek sanidine $^{40}\text{Ar}/^{39}\text{Ar}$ standard. *Quaternary Geochronology*, 39,
 887 205-213.
 888



- 889 Nomade, S., Muttoni, G., Guillou, H., Robin, E. & Scardia, G. First $^{40}\text{Ar}/^{39}\text{Ar}$ age of
 890 the Ceprano man (central Italy). *Quat. Geochronol.* **6**, 453-457 (2011).
 891
 892 Palombo, M.R., Magri, D., Molinari, D., Pisano, V., 2000-2002. The Pleistocene
 893 sequence of Campo del Conte (Lower Sacco Valley, southern Lazio). *Geologica*
 894 *Romana*, **36**, 289-309.
 895
 896 Patacca, E., Sartori, R., Scandone, P., 1990. Tyrrhenian basin and apenninic arcs:
 897 kinematic relations since late Tortonian times. *Memorie della Società Geologica*
 898 *Italiana* **45**, 425-451.
 899
 900 Pereira, A. *et al.* Geochronological evidences of a MIS 11 to MIS 10 age for several
 901 crucial Acheulian sites from the Frosinone province (Latium, Italy):
 902 Archaeological implications. *Quaternary Science Reviews* **187**, 112-129 (2018).
 903
 904 Pereira, A., Monaco, L., Marra, F., Nomade, S., Gaeta, M., Leicher, N., Palladino,
 905 D.M., Sottili, G., Guillou, H., Scao, V., Giaccio, B., 2020. Tephrochronology of the
 906 central Mediterranean MIS 11c interglacial (~425-395 ka): new constraints from
 907 Vico volcano and Tiber delta, Central Italy. *Quaternary Science Reviews* **243**:
 908 106470.
 909
 910 Sani, F., Del Ventisette, C., Montanari, D., Coli, M., Nafissi, P., & Piazzini, A.
 911 (2004). Tectonic evolution of the internal sector of the Central Apennines,
 912 Italy. *Marine and petroleum geology*, **21**(10), 1235-1254.
 913
 914
 915
 916